# Design concept of a $\gamma$-ray beam with low bandwidth and high spectral density

P. Constantin,* C. Matei, and C. A. Ur

*Extreme Light Infrastructure-Nuclear Physics (ELI-NP), "Horia Hulubei" National Institute for Physics and Nuclear Engineering, 30 Reactorului Street, 077125 Magurele, Ilfov, Romania*

(Received 27 November 2023; accepted 12 February 2024; published 28 February 2024)

The Variable Energy Gamma facility of the Extreme Light Infrastructure-Nuclear Physics center will deliver a gamma beam generated by the Compton scattering of laser and electron beams. It will have the highest spectral density and the lowest bandwidth available worldwide. A suite of several experimental setups is being developed for a wide range of research programs in fundamental and applied nuclear science driven by gamma beams. The proposed design concept for this facility is outlined. A study of the gamma beam properties at its source, as well as those after collimation, is presented. The impact of the variation in the parameters of the electron and laser beams on the quality of the gamma beam is analyzed and discussed.

DOI: 10.1103/PhysRevAccelBeams.27.021601

## I. INTRODUCTION

The Extreme Light Infrastructure-Nuclear Physics (ELI-NP) research center for nuclear photonics [1] has recently opened access to the user community at its state-of-the-art dual 100 TW and 1 PW laser beamlines [2]. The commissioning of its flagship two-arm 10 PW laser beamlines reaching intensities around $10^{23}\,\mathrm{W\,cm^{-2}}$, which are the most powerful lasers worldwide, is ongoing.

The extreme photon intensity of the high-power laser systems will be complemented by the high-energy gamma source of the Variable Energy Gamma (VEGA) facility. Designed to be the gamma beam with the highest spectral density and the lowest bandwidth, VEGA will be the next step in the field of high resolution studies of nuclear excitations.

Nuclear reactions induced by quasimonochromatic real photons are of special interest due to their high selectivity of the initial states participating in the reaction [3]. A fundamental reason lies in the well-defined angular momentum that is transferred during the photon absorption. For example, real photons excite only states with spin and parity $J^\pi = 1^-, 1^+$ and, to a lesser degree, $2^+$ in even-even and odd-A nuclei. Another reason comes from the development of $\gamma$ sources with high-energy resolution $\Delta E/E < 1\%$ and polarization degrees above 90%.

There are several methods to generate quasimonochromatic $\gamma$ beams. Examples are sources based on tagged photon bremsstrahlung and in-flight positron annihilation. However, the method that produces the highest quality $\gamma$-ray beams uses the process of Compton backscattering (CBS) of laser photons on relativistic electrons [3]. The double Lorentz boost of the photon increases its energy by a factor of $4\gamma_e^2$, where $\gamma_e$ is the electron relativistic factor and produces a tight energy-angle correlation centered on the electron direction.

The VEGA facility will consist of a warm linac that accelerates electrons to relativistic energies and injects them in an electron storage ring (ESR) where they collide at high frequency with laser photons inside a resonant optical cavity (ROC) [4]. The inherently high-forward focusing of this $\gamma$-ray beam, with an angular divergence below 1 mrad, is increased by selecting only the low-angle, high-energy component with a collimation system.

ELI-NP has developed several experimental setups to be used with the VEGA beamline. Fundamental nuclear physics is very well represented among these experimental programs with dedicated setups for nuclear resonance fluorescence [5], photonuclear reactions above the neutron separation threshold [6], nuclear astrophysics studies [7], and photofission and exotic nuclei research [8]. ELI-NP also has a diverse applied research program comprising setups for medical [9] and industrial studies [10]. A secondary positron beamline is developed for material science applications [11].

The first step in the design of the VEGA beamline is the analysis of the electron and laser beam parameters needed for the generation of a $\gamma$-ray beam with a given set of specifications. A software program that computes the CBS interaction between electron and laser beams, followed by

*Corresponding author: paul.constantin@eli-np.ro

*Published by the American Physical Society under the terms of the Creative Commons Attribution 4.0 International license. Further distribution of this work must maintain attribution to the author(s) and the published article's title, journal citation, and DOI.*

the collimation of the outgoing photons, has been implemented. Apart from its use in describing the $\gamma$-ray beam, this program will be an essential tool for the entire ELI-NP user community of setup designers, experiment developers, and data analyzers as a $\gamma$ generator for photonuclear physics simulations. This tool must accommodate for the specificity of all research programs since they require sampling of different regions in the gamma beam phase space when simulating different reaction types and the response of various detectors.

The main purpose of the work presented here is to study the relationship between the properties of the $\gamma$-ray beam with those of the electron and laser beams at their interaction point (IP), also referred to as the $\gamma$ source, and with those of the collimation system. The desired $\gamma$-ray beam specifications are described in Sec. II, together with the full set of beam parameters and their relationships. Section III details the main constructive and operational concepts envisaged at VEGA and, based on them, proposes the main parameters at the IP for the ESR and ROC components. Section IV follows with a description of the software used in the analysis of the $\gamma$-ray beam properties. Section V studies the tuning of the main VEGA parameters at the source and after collimation. An evaluation of the sensitivity of the VEGA specifications to deviations of the electron and laser beam parameters is presented in Sec. VI.

## II. VEGA DESIGN SPECIFICATIONS AND OPERATIONAL PARAMETERS

The design specifications of the VEGA system, established in accordance with the requirements of the above research programs, are listed in Table I. A comparison of the main parameters at VEGA and other CBS facilities is made in Table II. The next paragraph defines these parameters, with examples of how they are calculated to follow in Secs. IV and V.

The energy spectrum is tunable in the 1–20 MeV range by adjusting its maximum via the electron beam energy and its minimum via collimation, as described below. The bandwidth BW is the ratio between the FWHM (full width at half maximum) of the energy spectrum after collimation and its peak energy $E_\gamma^{\max}$. The linear polarization $\xi$ is the component of the gamma Stokes vector along the polarization direction of the laser photon, considered here to be vertical. The angular divergence $D_\theta$ is the FWHM of the polar angle distribution after collimation. The beam spot $D_x$ is the FWHM of the one-dimensional transversal distribution at a reference point located 10 m downstream from the $\gamma$ source, immediately after the collimation system, hence $D_x = D_\theta \times 10$ m.

The total intensity $I$ is the total rate of $\gamma$s emitted at the source. The total flux $F$ is the total rate of $\gamma$s selected by the collimation system. Therefore, $F$ is $I$ in the beam spot and in the bandwidth. The spectral density SD in the energy peak is the total flux $F$ divided by the energy spectrum FWHM. The off-peak spectral density OSD is the total flux in the beam spot, hence after collimation, but with energy outside the bandwidth. An ideal collimation system has a null OSD, therefore, this quantity estimates the background generated by collimation.

TABLE I. Design specifications of the VEGA system.

| Name | Symbol | Specification |
|---|---|---|
| Maximum energy | $E_\gamma^{\max}$ | $\leq$20 MeV |
| Bandwidth | BW | $\leq$0.5% |
| Polarization | $\xi$ | $\geq$95% |
| Divergence | $D_\theta$ | $\leq$0.15 mrad |
| Beam spot | $D_x$ | $\leq$1.5 mm |
| Total intensity | $I$ | $\geq 10^{11}$ $\gamma$/s |
| Total flux | $F$ | $\geq 4 \times 10^8$ $\gamma$/s |
| Peak spectral density | SD | $\geq 5 \times 10^3$ $\gamma$/s/eV |
| Off-peak spectral density | OSD | $\leq 10^{-2}$ $\gamma$/s/eV |

For given electron and laser beams, collimation is the handle to find an optimal $\gamma$ beam since it allows us to improve some parameters at the expense of others. For example, tighter collimation not only improves the bandwidth and the beam spot but also decreases the total flux. The variation of the spectral density by collimation is nontrivial, since this quantity is a ratio of two parameters that both decrease by collimation, namely the total flux $F$ and the energy peak FWHM.

Most nuclear photonics studies are related to properties of various types of nuclear excitations, like single particle or collective states, either by themselves in structure studies or as initial states in reaction studies. Hence, the usual $\gamma$ beam optimization revolves around the BW and $F$ parameter couple, in the sense that a decrease of the bandwidth down to the energy resolution necessary to resolve these states is desired, but at the same time keeping the number of $\gamma$s in the energy peak as high as possible in order to preferentially populate them. The maximum spectral density SD captures the outcome of this optimization, hence it is regarded as the main parameter in nuclear photonics research. The necessary energy resolution is given by the level density in the region of interest. Generically speaking, the nuclear level density not only increases with the excitation energy but also depends strongly on the nuclear shell structure around the valence nucleons.

To describe the energy tuning procedure, let us consider the CBS energy-angle equation, which is derived from the conservation of energy and momentum. For head-on photon-electron collisions and in the approximation of small scattering angles $\theta_\gamma \ll 1$ and relativistic electrons $\gamma_e \gg 1$, it reads

$$E_\gamma \approx \frac{4\gamma_e^2 E_l}{1 + (\gamma_e \theta_\gamma)^2 + 4\gamma_e^2 E_l / E_e}, \tag{1}$$

TABLE II. Comparison between the main gamma beam parameters at VEGA and other CBS facilities: energy range $E$, bandwidth BW, total intensity $I$ at source, total flux $F$ on target or after collimation, and spectral density SD. Three dots are used where the parameter value is not available. A reference is given in the last column for further details.

| Facility | Location | $E$ (MeV) | BW (%) | $I$ ($\gamma$/s) | $F$ ($\gamma$/s) | SD ($\gamma$/s/eV) | Ref. |
|---|---|---|---|---|---|---|---|
| VEGA | ELI-NP Romania | 0.2–20 | 0.5 | $10^{11}$ | $4\times10^{8}$ | $5\times10^{3}$ | … |
| HI$\gamma$S | Duke USA | 1–158 | 0.8–10 | $3\times10^{9}$ | $5\times10^{8}$ | $10^{2}$ | [12] |
| SLEGS | Shanghai China | 0.4–22 | 1–4 | $10^{10}$ | $10^{5}$–$10^{7}$ | $10^{2}$ | [13] |
| NewSubaru | RCNP Japan | 0.5–76 | 1–2 | $10^{9}$ | $2\times10^{6}$ | $10^{2}$ | [14] |
| LEPS | RCNP Japan | 1500–2900 | 1.25 | … | $5\times10^{6}$ | 0.1–0.3 | [15] |
| CLS | Saskatoon Canada | ≤15 | 0.1 | $10^{10}$ | … | $10^{3}$ | [16] |
| GRAAL | Grenoble France | 550–1500 | 1.1 | … | $3\times10^{6}$ | … | [17] |
| ROKK-1M | Novosibirsk Russia | 100–1600 | 1–3 | … | $10^{6}$ | … | [18] |

where the $e$, $l$, $\gamma$ indices denote electron, laser photon, and gamma photon quantities, respectively.

At high-electron relativistic factor $\gamma_e \approx E_e/m_e c^2$, a tight $E_\gamma(\theta_\gamma)$ anticorrelation results from Eq. (1). Backscattered $\gamma$s have the maximum energy

$$E_\gamma^{\max} = E_\gamma(\theta_\gamma = 0) = \frac{4\gamma_e^2 E_l}{1 + 4\gamma_e^2 E_l/E_e} \approx 4\gamma_e^2 E_l, \quad (2)$$

and, at fixed laser photon energy $E_l = hc/\lambda$, this maximum energy is controlled via the electron energy $E_e$. After both $E_l$ and $E_e$ are set, the minimum energy $E_\gamma^{\min}$ is set by collimation $\theta_\gamma \le \theta_{\text{coll}}$. The above approximate equations in the laboratory reference frame will be replaced in Sec. IV by an exact equation in the electron rest frame.

The total $\gamma$ intensity $I$ is the product between the Thomson cross section $\sigma_T = 0.667$ b, the single collision luminosity $L_{\text{sc}}$, the number of electrons in a beam bunch $N_e$, the number of photons in a laser pulse $N_l$, and the bunch-pulse collision frequency $f$:

$$I = \frac{N_\gamma}{t} = \sigma_T L_{\text{sc}} N_e N_l f, \quad (3)$$

where $N_e = Q/e = I_e/(ef)$ with $I_e$ and $Q$ the electron current and bunch charge, and $N_l = E_L/E_l = P_L/(E_l f)$ with $P_L$ and $E_L$ the laser power and pulse energy. The single collision luminosity depends on the transversal dynamic properties of the two beams [19]:

$$L_{\text{sc}} = \frac{1}{2\pi(\sigma^2 + \sigma_l^2)}, \quad (4)$$

where $\sigma \equiv \sigma_x = \sigma_y$ and $\sigma_l \equiv \sigma_{xl} = \sigma_{yl}$ are the transversal position rms of the electron and laser beams, respectively. Throughout this article, the electron and laser beams are assumed to be round (symmetric) at the IP.

If the two beams cross at some angle $\delta$, the single collision luminosity decreases by the factor

$$\frac{L_{\text{sc}}(0)}{L_{\text{sc}}(\delta)} = \sqrt{1 + \frac{\sigma_z^2 + \sigma_{zl}^2}{\sigma^2 + \sigma_l^2}\tan^2\left(\frac{\delta}{2}\right)}, \quad (5)$$

where $L_{\text{sc}}(0)$ is given by Eq. (4), and $\sigma_z$ and $\sigma_{zl}$ are the longitudinal position rms of the electron and laser beams.

The transversal position rms $\sigma$ and the transversal angular rms $\sigma'$ of the electron beam are related to its emittance $\epsilon$ and Twiss parameters $\beta$ and $\gamma$:

$$\sigma = \sqrt{\epsilon\beta}, \qquad \sigma' = \sqrt{\epsilon\gamma}. \quad (6)$$

The $\sigma$ and $\sigma'$ parameters are also known as the beam waist and the beam divergence, respectively, while $\beta$ is also known as the $\beta$ function. The $\beta$ and $\gamma$ Twiss parameters are related via the third Twiss parameter $\alpha$:

$$\beta(s)\gamma(s) = 1 + \alpha^2(s), \quad (7)$$

where $\alpha(s)$ quantifies the position-angle correlation at point $s$ on the beam axis. If $\alpha(s_0) = 0$, where $s_0$ is the IP location, then Eq. (6) at the $\gamma$ source $s = s_0$ becomes

$$\sigma = \sqrt{\epsilon\beta}, \qquad \sigma' = \sqrt{\epsilon/\beta}. \quad (8)$$

An important equation, derived in Ref. [20], decomposes the $\gamma$ beam rms bandwidth in its main components, namely the electron and laser energy spreads, the collimation energy selection, and the electron angular spread:

$$\left(\frac{\delta E_\gamma}{E_\gamma}\right)^2 \approx 4\left(\frac{\delta E_e}{E_e}\right)^2 + \left(\frac{\delta E_l}{E_l}\right)^2 + \frac{\gamma_e^4\theta_{\text{coll}}^4}{12} + 4\gamma_e^4\sigma'^4. \quad (9)$$

Equations (4) and (9) require minimal $\sigma$ and $\sigma'$ simultaneously. Equation (8) translates this into an emittance as small as possible, but the optimal $\beta$ value is indefinite. In practice, when a very small emittance is attained, larger $\beta$ values are used to achieve the above requirements.

For the laser beam, its transversal position rms $\sigma_l$ is related to the wavelength $\lambda$ and Rayleigh range $\beta_0$:

$$\sigma_l = \sqrt{\frac{\lambda\beta_0}{4\pi}}. \quad (10)$$

## III. VEGA DESIGN OPERATIONAL CONCEPTS

CBS gamma facilities can have the IP at the focus of the electron linac or inside an ESR fed by the linac. While the first option presents some advantages, notably the fact that the electron beam does not need to be reconditioned, most facilities use an ESR. The most important benefit comes from the accumulation of many electron bunches, which are circulated at several MHz, resulting in a very high collision frequency. For example, HI$\gamma$S can store as many as 64 bunches circulated at 2.8 MHz, leading to a collision frequency of $f = 179$ MHz [12]. Therefore, using an ESR leads to a $\gamma$ source with very high intensity without placing strong requirements on the linac. In particular, the bunch frequency is quite low since the purpose of the linac is to inject bunches into the ESR at the rate necessary to replace the beam losses there. Other important benefits include beam cooling control by synchrotron radiation inside the ESR, which allows for high-quality steady-state electron beams at the IP, like low emittance, and the mode locking at high frequency between the electron beam and the laser ROC.

Following the above design concept, the VEGA system [4] uses an rf electron gun to generate electron bunches, accelerates them to energy $E_e$ in a linac, and injects them in an ESR where they are circulated at high frequency $f_b$. The number of stored bunches $N_b$ and their circulation frequency $f_b$ make the collision frequency $f = N_b \times f_b$. At the same time, a continuous wave laser at wavelength $\lambda$ feeds an ROC, which resonantly amplifies its power $P_L$ and generates pulses with frequency $f$ matching that of the electron bunches. The ESR has two straight sections, one for linac injection and the other for the $\gamma$ source, and two curved sections. Electromagnetic devices align the two beams to collide at a very shallow crossing angle $\delta$.

Although CBS at nonzero $\delta$ leads to a decrease in luminosity according to Eq. (5), this interaction configuration is actually desirable. One reason is that the laser mirrors are not hit by the $\gamma$-ray beam and the ROC is not exposed to the synchrotron radiation. Also the formation of secondary low-intensity IPs between the laser and electron beams, away from the main IP, is avoided. The luminosity decrease due to the crossing angle is kept at a level below 1% by tuning the ratio between the longitudinal and transversal position rms of the two beams.

The parameters of the electron and laser beams are established considering the required $\gamma$-ray beam specifications listed in Table I, the parameter relationships detailed in Sec. II, and the design considerations discussed in this section. Also the design choices made at the other modern CBS gamma facilities using storage rings listed in Table II provided important guidance. This is especially the case for HI$\gamma$S, SLEGS, and NewSubaru, which have many similarities with VEGA.

The emittance in an ESR decreases exponentially, due to the synchrotron radiation in its curved sections [21], with a damping time strongly dependent on the electron energy $E_e$:

$$\epsilon(t) = \epsilon(0)e^{-t/\tau}, \qquad \tau = \frac{T}{CE_e^3}, \tag{11}$$

where $T = 1/f_b < 1$ μs is the turn time and $C$ is a constant of the ESR beamline with different values for the vertical and horizontal directions. The limit to this decrease is set by quantum excitations. Hence, ESRs use synchrotron radiation damping to minimize their emittance, a very effective method at high energies.

Additionally, the beam energy spread $\delta E_e$, emittance $\epsilon$, and bunch length $\sigma_z$ are energy dependent and correlated due to the intrabeam scattering (IBS) process. At constant bunch charge $Q$, the IBS effects grow quickly and become important at low $E_e$ and small $\sigma_z$. Up to some level, these effects can be moderated by increasing $\sigma_z$ via changes of the rf cavity frequency and amplitude. A consequence of the $\delta E_e$ and $\epsilon$ growth at low $E_e$ is that the bandwidth becomes dominated by $\delta E_e$ and $\sigma'$, hence stronger collimation has little influence [see Eq. (9)].

These low energy effects can be avoided by doubling $\lambda$ once $E_e$ has decreased by $\sqrt{2}$ and restarting from the initial electron energy. This method limits the minimum ESR energy in order to maintain the synchrotron radiation damping for superior beam parameters. At VEGA, the maximum energy $E_\gamma^{\max} = 20$ MeV is obtained for a green laser with $\lambda = 530$ nm (2.34 eV), which is the green spectrum middle, and $E_e = 757$ MeV. $E_\gamma^{\max}$ values down to 10 MeV are generated by decreasing $E_e$ to 535 MeV at the same $\lambda$. For energies below 10 MeV, an infrared (IR) laser with twice wavelength $\lambda = 1060$ nm (1.17 eV) is used and the electron energy range is reset from 753 to 531 MeV, reaching $E_\gamma^{\max} = 5$ MeV.

The study presented here uses the above method and stops at a $\gamma$ energy of 5 MeV, corresponding to an electron energy of 531 MeV. Hence, emittance is kept at a low value by fast synchrotron radiation damping, and the IBS effects that make $\delta E_e$ and $\epsilon$ energy dependent are small. Also the effect of adiabatic damping, which makes $\epsilon \sim 1/E_e$ [22], on emittance variation is kept at a level below 30%. Obviously, going below this $\gamma$ energy can be done by doubling the wavelength again. Alternatively, the IR laser can be used further, say to $E_\gamma^{\max} \approx 1$ MeV corresponding to $E_e = 236$ MeV, by applying correction techniques, like the one increasing $\sigma_z$ mentioned above and accepting a higher emittance and energy spread.

Another option for ESRs at low energy is an additional emittance damping via radiative laser cooling, which is very effective against IBS effects [23]. It involves the use of a second laser with a high pulse energy of ~1 J and short Rayleigh range of ~1 mm, aligned with the electron beam in the straight ESR section where the linac bunches are injected. Considering also the need for a chromaticity

TABLE III. Beam parameters for the ESR electron bunches and ROC laser pulses at the IP of the VEGA $\gamma$ source are listed in the third row; the two values for $\sigma_l$ and $P_L$ correspond to the two values for $\lambda$. The fourth row lists the corresponding values proposed for the $\gamma$ source in Ref. [24]; the two values for $\beta$, $\sigma$, and $\sigma'$ correspond to the $x$ and $y$ transversal components.

| ESR electron bunches | | | | | | | ROC laser pulses | | | | | CBS collision | |
|---|---|---|---|---|---|---|---|---|---|---|---|---|---|
| $Q$ (nC) | $\epsilon$ (nm) | $\beta$ (m) | $\sigma$ (μm) | $\sigma'$ (μrad) | $\sigma_z$ (mm) | $\delta E_e$ (%) | $\lambda$ (nm) | $\beta_0$ (m) | $\sigma_l$ (μm) | $\sigma_{zl}$ (ps) | $P_L$ (kW) | $f$ (MHz) | $\delta$ (mrad) |
| 1 | 2 | 10 | 141 | 14 | 10 | 0.05 | 530/1060 | 1 | 205/290 | 15 | 36.5/30.2 | 70 | 5 |
| 0.25 | 0.42 | 0.70/0.63 | 17.2/16.4 | 28.1/25.8 | 0.271 | 0.044 | 515 | 0.0048 | 14 | 1.5 | 0.64 | 0.0032 | 140 |

correction due to the increased energy spread, this method is left as a future upgrade option for VEGA.

Table III shows the set of beam parameters at the IP and their energy independent values used for the simulation of all $\gamma$ beam configurations. A collision frequency of $f = 70$ MHz, remaining to be split into $N_b$ and $f_b$ during the ESR design, is considered feasible. The high $\gamma$ source intensity $I$ is obtained mainly via large $f$ and $P_L$ values. This allows us to keep the bunch charge at the relatively low value of $Q = 1$ nC to simplify its acceleration, injection, and storage at high circulation frequency.

The proposed value for the emittance is $\epsilon = 2$ nm, which is slightly below the 4–40 nm range at the other CBS $\gamma$ facilities, but in line with the current capabilities of the latest ESR facilities [21]. Relying on this low emittance, a large $\beta = 10$ m is set in order to get a small $\sigma' = 14$ μrad, but still have also a reasonable $\sigma = 141$ μm, as discussed in Sec. II. The longitudinal bunch length of $\sigma_z = 10$ mm is small enough to keep the luminosity decreasing due to the $\delta = 5$ mrad crossing angle being negligible.

A $\delta E_e = 0.05\%$ value is set for the electron energy spread, considering Eq. (9), the BW $\leq 0.5\%$ specification, and the range of values for the other parameters. Then the maximum bandwidth at $E_e = 757$ MeV, expressed in terms of rms widths, is composed from the components $2\delta E_e/E_e = 0.1\%$, $2\gamma_e^2\sigma'^2 = 0.09\%$ and $\gamma_e^2\theta_{\rm coll}^2/\sqrt{12} = 0.23\%$ and 0.32% for $\theta_{\rm coll} = 60$ and 71 μrad, respectively. These choices for the collimation angle will be explained in Sec. IV. B. Summing up, the rms bandwidth at maximum electron energy is $\delta E_\gamma/E_\gamma = 0.26\%$ and 0.35% for the two collimation angles. Note that the dominant component is that generated by collimation, which is a desirable feature of the $\gamma$ beamline since it provides maximum flexibility in tuning its parameters.

The Rayleigh range of $\beta_0 = 1$ m produces a laser beam with transversal position rms $\sigma_l = 205,\ 290$ μm [see Eq. (10)] of similar size as the electron beam. The longitudinal pulse length $\sigma_{zl} = 15$ ps $= 4.5$ mm is chosen to minimize the luminosity decrease in Eq. (5) and to keep it smaller than the longitudinal bunch length $\sigma_z$ for optimal overlap. The values for the laser ROC amplification power $P_L$, which is used to tune directly the $\gamma$ source intensity, will be discussed in Sec. V. A. These laser pulses have small energies $E_L = P_L/f = 0.43$–$0.52$ mJ and large sizes $\pi\sigma_l^2 c\sigma_{zl} = 0.59$–$1.19$ mm$^3$, leading to very small intensities $I = 1.1$–$2.6 \times 10^8$ W/mm$^2$ at the IP.

Electrons are lost by interaction with the ROC pulses, via either radiative energy loss or CBS recoil, when their energy moves outside the energy spread $\delta E_e$. The ESR maintains the beam energy by removing electrons outside $E_e \pm \delta E_e$ and compensates by linac injection. Momentum correction is not considered here, since it depends on the ESR design.

The fractional radiative energy loss of one electron after passing through the laser pulse is given by Eq. 4 in Ref. [23]. Due to the small $E_L$ and large $\beta_0$ values, it is very small $\Delta E_e/E_e \approx (1.3$–$4.7) \times 10^{-9}$. Assuming a circulation frequency $f_b = 10$ MHz ($N_b = 7$ stored bunches), it adds up to $\delta E_e/E_e$ in 11–37 ms. Regarding the recoil energy loss, since it moves the electron energy outside $\delta E_e$ in most cases, we can estimate that up to $10^{11}$ e$^-$/s are lost. Hence, out of the total charge stored $N_b \times Q = 7$ nC, about 2.5% is lost in 11 ms. Concluding, without momentum correction, a linac injection at less than 10 ms (>100 Hz) is needed.

These moderate transverse spot sizes of 100–300 μm and longitudinal lengths of 5–10 mm, made possible by very high $f$ and $P_L$ and low $\epsilon$ values, are crucial for easier beam focusing and synchronization at the IP.

An earlier design proposed for the $\gamma$-ray beam at ELI-NP is presented in Ref. [24] and had the IP at the linac focus. Its main parameters are also listed in Table III for comparison. It has a much smaller collision frequency and laser power. To reach the same $\gamma$-ray beam intensity, it compensates with much smaller beam sizes, in both transversal and longitudinal dimensions and for both electron bunches and laser pulses, by at least an order of magnitude. This is done with a very small emittance and drastic decreases of $\beta$ and $\beta_0$. Obtaining such a small emittance without the radiation damping employed at ESRs [21] could prove to be a big challenge. Also the spatial overlap and temporal synchronization of electron bunches and laser pulses with sizes of several microns is very difficult. Note also that the parameters in Table III meet the specifications in Table I at $E_e = 530$ MeV ($E_\gamma = 10$ MeV). However, when they are used at higher energies, the bandwidth increases steadily above 0.5% [according to Eq. (9)], requiring a further $\epsilon$ reduction. Specifically, at $E_e = 747$ MeV ($E_\gamma = 20$ MeV) and for a minimal $\theta_{\rm coll} = 30$ μrad, Eq. (9) requires an emittance of $\epsilon = 0.03$ nm.

After defining the parameters of both beams at the IP, the simulation program that generates the $\gamma$ beam from beam-beam CBS is used to study its properties.

## IV. GAMMA BEAMLINE SIMULATION SOFTWARE

Several CBS simulation programs are available [20,24–29], the most popular being CAIN [30]. A customized CBS program has been developed for the VEGA facility in order to optimize its performance, closely control the implementation of the physical processes, and easily connect to the other simulation modules.

The simulation software is incorporated within the GEANT4 C++ library [31]. This framework choice is motivated by its widespread use within the nuclear physics community in general and the VEGA user community in particular, and by its intended future use as an event generator for simulations of experimental setups and programs at VEGA. The program comes as two separate classes: the first for the Monte Carlo generation of $\gamma$s via electron-laser beam-beam Compton scattering, and the second for their transport through the collimation system which produces the final gamma beam.

### A. Beam-beam Compton backscattering

The class that simulates the $\gamma$ source, called *GammaGenerator*, takes as input the parameters of the electron and laser beams at the IP and generates $\gamma$s in the GEANT4 format. Only the main features are discussed in this sub-section. A full description of this class is given in the Appendix. It uses the CLHEP C++ library [32] of space (3D) and Lorentz (4D) vectors and transformations to define all particle states and their modifications.

The electron position and four-momentum vectors are generated using the input electron beam parameters. Then a photon is assumed to exist at the electron position, and its four-momentum and polarization vectors are generated using the input laser beam parameters. Hence, for each electron generated, there will be one outgoing photon and the user specifies how many of them to be produced in a particular run. To recover the proper normalization of the generated distributions, the total intensity $I$, or $\gamma$ event rate, is computed separately according to Eqs. (3)–(5). Its value must be used to scale any output distribution dependent on the gamma beam intensity.

The above scaling method departs from the beam sampling methods usually employed by CBS programs. The advantage is a large execution speedup, a highly desirable feature for an event generator to be used in extensive setup simulations. The generation of 10 million $\gamma$s takes 217 s on one thread of an Intel i7-4710MQ 2.5 GHz processor. Many-particle interactions, like those between the electrons in the bunch (IBS effects) or those between the electron and multiple photons in the laser pulse (nonlinear CBS), cannot be implemented in this method, except when these interactions are expressed as modifications of the electron properties using concepts like effective field or dressed mass. For the experimental programs planned at VEGA, this trade-off is very useful.

After the electron and photon initial states are generated, the Compton scattering proceeds as usual. First, all vectors are boosted to the electron rest frame and the photon is aligned on $+z$. Working in this reference frame simplifies significantly all equations. For example, the exact energy-angle equation, equivalent to the approximate Eq. (1) in the laboratory frame, becomes

$$\frac{1}{E_\gamma} = \frac{1}{E_l} + \frac{1-\cos(\theta_\gamma)}{m_e c^2}, \tag{12}$$

where $E_\gamma$ and $\theta_\gamma$ are the gamma energy and emission angle, and $E_l$ is the photon energy. The outgoing $\gamma$ is generated using the Compton cross section in the electron rest frame and boosted back to the laboratory frame.

This class uses equations compiled from Refs. [12,19,21,22,25,30,33,34] and makes two additional assumptions: (i) the electron and laser beams have the Gaussian space-time structure described by the parameters detailed in Sec. II and no distortions, like satellite peaks, halo particles, or tails, are present and (ii) the two beams are perfectly synchronized, hence electron bunches and laser pulses overlap at their centers when they collide.

### B. Collimation system

The second component of the VEGA beam simulation tool is a method, called *CollimationSystem*, of the standard GEANT4 class *DetectorConstruction*. It is a software implementation of the designs of the two $\gamma$ beam collimation systems developed at ELI-NP.

The first system, shown in Fig. 1, allows for the collimation of the $\gamma$ source with a set of six apertures. Its components, in order from the $\gamma$ source IP, which is located at 7.7 m to the right, are (i) rectangular motorized beam stopper, shown in blue, made of 20 cm thick tungsten with a 5 mm hole; (ii) cylindrical neutron shield, shown in yellow, made of 20 cm thick borated polyethylene with a 25 mm hole; (iii) cylindrical precollimator, shown in pink, made of 10 cm thick lead with a 10 mm hole; (iv) shielding wall made of concrete, not shown in Fig. 1, with a penetration in which the neutron shield and the precollimator are encapsulated; and (v) beam collimator, shown in green, a stack of 20 tungsten plates with 1 cm thickness and 1 cm gaps.

A vacuum beam pipe with Kapton windows covers the distance between the exit window of the ROC around the IP and the beam stopper. The spaces between all of the above components of the collimation systems are filled with air. The materials and dimensions of these components were chosen to fulfill the radiological protection requirements for the ELI-NP project.

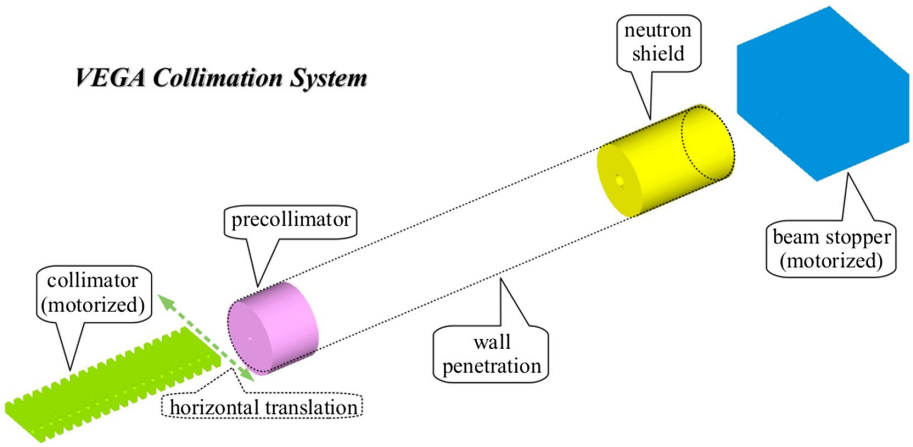


FIG. 1. Visualization from GEANT4 of the VEGA collimation system: the beam stopper in blue, the neutron shield in yellow, the precollimator in pink, and the primary beam collimator in green. The interaction point is at 7.7 m on the right side.

The beam collimator can translate horizontally, via remote controlled motors, in order to align one of its seven circular apertures with the axis from the $\gamma$ source through the system components. The distance from the IP to the first collimator plate is 9.1 m. The diameters of these apertures are $a = 0.5, 0.7, 0.9, 1.1, 1.3, 3$, and 10 mm, corresponding to the collimation polar angles of $\theta_{\text{coll}} = 27, 38, 49, 60, 71, 164$, and 550 μrad. The smallest aperture has a diameter of 0.5 mm chosen based on the current capabilities of mechanical manufacturing and alignment. The next four apertures increase the radius in steps of 0.1 mm, corresponding to an increase of the collimation angle of 11 μrad. The last two apertures are significantly larger and are meant to be used when broad $\gamma$ beams are necessary for operations like alignment and calibration.

The inclusion of collimation in the simulation increases the execution time by more than an order of magnitude. The most computational resources are used for the interaction of the generated $\gamma$s with the collimator materials.

A more complex collimation system, which can vary continuously the angular acceptance of its aperture in the range of 60–700 μrad, has been developed for ELI-NP and is described thoroughly in Ref. [35].

For given gamma beam properties at the IP, the choice of the collimator aperture is the main control method for the beam divergence, bandwidth, and flux on targets.

## V. TUNING OF MAIN VEGA PARAMETERS

In this section, the software is used with the input parameters in Table III to obtain the VEGA specifications in Table I. The analysis is done for VEGA parameters at the IP, referred to as "source specifications," and after collimation, referred to as "beamline specifications."

### A. Source specifications

As mentioned above, the total intensity $I$ is obtained by tuning the laser ROC amplification power $P_L$. In particular, for the set of parameters established above, the intensity specification limit $I = 10^{11}$ $\gamma$/s is reached for $P_L = 36.5$ kW with the green laser. This value for $I$ contains the down correction of the single collision luminosity due to finite crossing angle in Eq. (5) and another down correction of the CBS electron-photon cross section, due to electron recoil [25]

$$\sigma_{ep} = \sigma_T \frac{(P_{e\mu} + P_{l\mu}) \cdot (P_e^{\mu} + P_l^{\mu})}{(m_e c^2)^2}, \tag{13}$$

where $\sigma_T$ is the Thompson cross section and $P_{e,l}^{\mu} = (E_{e,l}/c, \vec{p}_{e,l})$ are the electron and photon 4-momenta. The correction factor in Eq. (13) is averaged over all collisions in the simulation and applied to Eq. (3). The combined correction factor due to both effects is in the 3%–3.5% range, depending on the various parameters used for the $\gamma$ sources. When using the IR laser system, the changes in the pulse number of photons $N_l$ and transversal position rms $\sigma_l$ are compensated by the value for $P_L = 30.2$ kW in order to reach the same intensity specification limit. Optical cavities with higher amplifications are technologically possible [36], making an increase of the total intensity by up to an order of magnitude achievable.

Two other effects can change the $\gamma$ source parameters. The first is the hourglass effect, which leads to a luminosity reduction due to the variation of the transverse beam size along the bunch length. The magnitude of this reduction was estimated at $2 \times 10^{-5}$ using the formalism in Ref. [37], hence it is negligible. The second effect is the nonlinear Compton scattering that takes place at very high laser intensity when the electron interacts with more than one photon simultaneously and emits one gamma ($e^- + np \to e^- + \gamma$). For the ROC parameters considered here, the maximum normalized vector potential is $a_0 = 6.7 \times 10^{-5}$ for the IR laser, hence this last correction is also negligible [38].

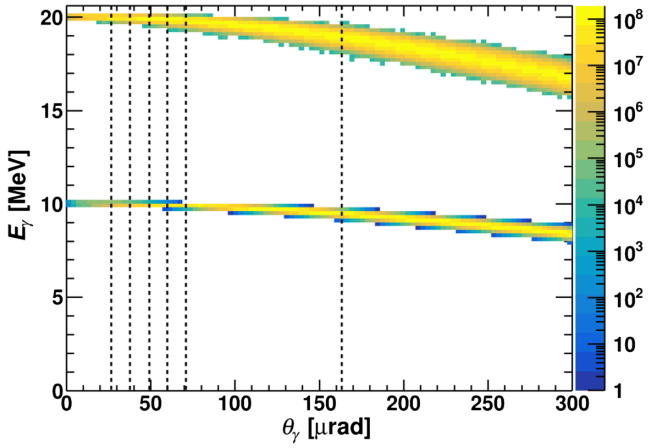


FIG. 2. Energy-angle correlation for the 20 and 10 MeV sources in the upper and lower distributions, respectively. The dashed lines show the first six collimation angles.

An important characteristic of CBS $\gamma$ sources is the tight correlation between energy $E_\gamma$ and polar angle $\theta_\gamma$ because it allows the formation of very narrow energy spectra by collimation. This correlation is shown in Fig. 2 for the maximum energies of 20 and 10 MeV in the upper and lower distributions, respectively. The logarithmic $z$ scale represents the number of $\gamma$s per second. An angle range up to 300 μrad is used to make visible the first six collimation angles described in Sec. IV.

Another important characteristic of a CBS $\gamma$ source is the almost perfect replication of the laser polarization. For a linearly polarized laser of 0.95 degree along the vertical axis, the correlation between the average $\gamma$ linear Stokes vector component $\xi$ and the polar emission angle $\theta_\gamma$ is shown in Fig. 3 up to 300 μrad. The six dashed lines show again the first six collimation angles. The first five angles recover $\xi = 0.95$ with negligible spread, while the sixth has an rms of 0.1% already. Only above $\theta_\gamma \gtrsim 150$ μrad, one can observe the start of a very slow decrease of $\xi$, accompanied by a slow spread increase. The inset in Fig. 3 shows the correlation between the $\gamma$ energy $E_\gamma$ and azimuthal angle $\phi_\gamma$ for the 20 MeV source. A strong and complex modulation around the laser polarization direction $\phi_l = 90°$ is visible at all energies, except the very lowest $E_\gamma \sim 0$ MeV and the highest $E_\gamma \sim 20$ MeV. Since collimation selects the very narrow energy band close to the maximum energy, uniform azimuthal angle distributions are recovered in the downstream $\gamma$ beamline. Typically, the azimuthal modulation starts to develop above $\theta_\gamma \gtrsim 150$ μrad for collimated $\gamma$-ray beams at all energies.

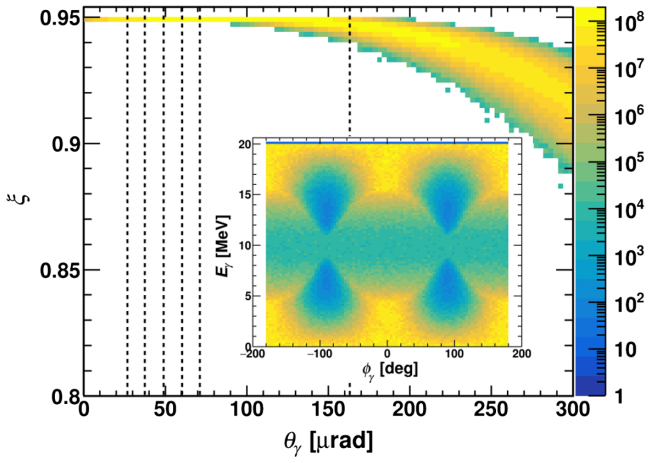


FIG. 3. The polarization-polar angle correlation for the 20 MeV source. The dashed lines show the first six collimation angles. The inset shows the energy-azimuthal angle correlation for the same source.

### B. Beamline specifications

Collimation by narrow apertures sets the minimum (threshold) energy and simplifies significantly the structures present in the $\gamma$ source at large emission angles. For example, the complex azimuthal modulation and polarization spreading shown in Fig. 3 is replaced by an isotropic distribution at fixed polarization in the corresponding $\gamma$ beamline. However, collimation also brings other background effects. This is due to the fact that, in reality, the collimation process is more complicated than the simple picture given in Figs. 2 and 3. Primary $\gamma$s that enter the apertures closest to the IP can scatter inside the intermediate apertures or can even penetrate the last ones. Additionally, primary $\gamma$s outside the apertures interact with the collimator material and generate secondary $\gamma$s and electrons.

Two background sources, which are not included in our software, come from the synchrotron radiation emitted by the electron beam and the bremsstrahlung radiation on beam pipe gas [39] passing through the collimator apertures. The addition of a very small, but finite, beam crossing angle is a direct method to reduce these components and should be adjustable in order to control it.

The resulting behavior of the $\gamma$ beamline at 20 MeV, after collimation with the apertures of 0.5 and 1.1 mm, is shown in Fig. 4. The black dashed lines show the corresponding collimation angles, while the red dotted lines show the energy interval for an FWHM of 0.1 MeV due to the BW = 0.5% specification. A logarithmic $z$ axis is again chosen to bring forth the outliers. The small number of primary $\gamma$s in each panel that is above the black dashed line has an emission angle $\theta_\gamma$ at the IP larger than the collimation angle of the aperture farthest away from the IP. Their presence in the collimated beamline is due to the effects mentioned above. These $\gamma$s contribute to the energy spectrum both under the main peak, where they increase the flux without increasing the bandwidth, but also in the low energy tail, where the flux increase is accompanied by a bandwidth increase.

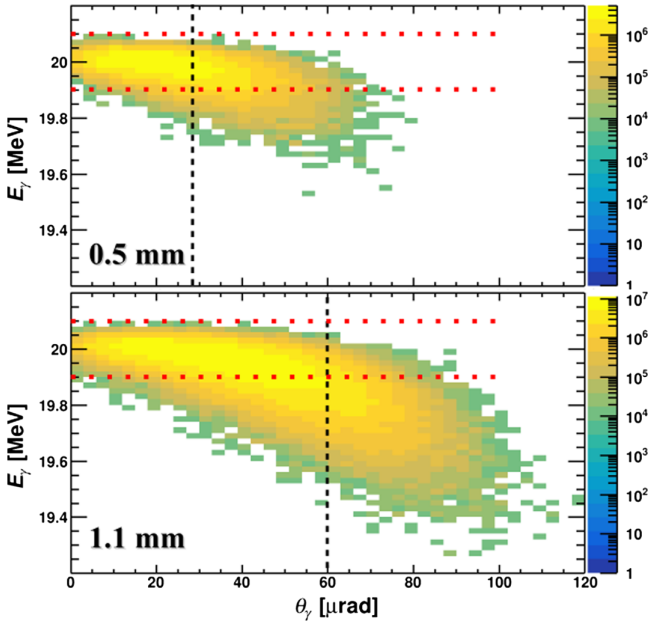


FIG. 4. Energy-angle correlation for the 20 MeV beamline after passing through the collimation system with the apertures of 0.5 and 1.1 mm. The vertical black dashed lines show the corresponding collimation angles, while the horizontal red dotted lines show the BW specification.

Selected examples of the energy spectra corresponding to the beam parameters in Table III, normalized to $I = 10^{11}$ $\gamma$/s, are shown in Figs. 5 and 6. The first figure demonstrates the effect of enlarging the collimation aperture for the 20 MeV beamline: both the bandwidth BW and the flux $F$ in the beam spot increase. The second figure demonstrates the effect of the Lorentz boost by keeping the collimation aperture fixed at 0.7 mm and increasing the energy: the range of $\gamma$ energies passing through the collimator increases.

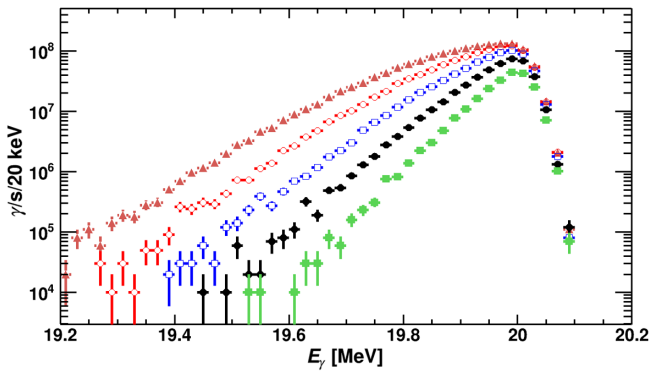


FIG. 5. Dependence of the energy spectra for the 20 MeV beamline on the aperture of the collimation system: 0.5 mm (full green squares), 0.7 mm (full black circles), 0.9 mm (open blue squares), 1.1 mm (open red circles), and 1.3 mm (full brown triangles). The vertical bars show statistical errors and the horizontal bars show the bin width.

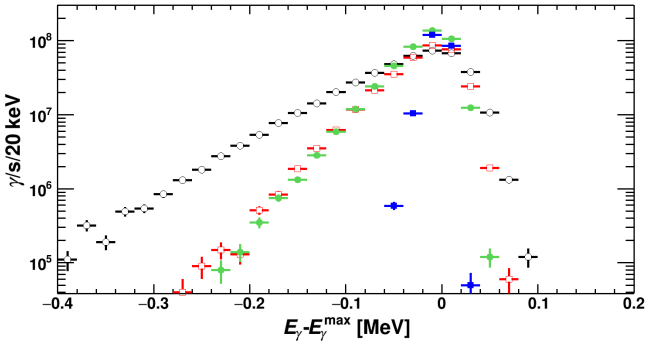


FIG. 6. Energy spectra, relative to the maximum energy, of the 5 MeV (full blue squares), 10 MeV (full green circles), 15 MeV (open red squares), and 20 MeV (open black circles) beamlines after collimation with the 0.7 mm aperture. The vertical bars show statistical errors and the horizontal bars show the bin width.

Although Eqs. (1) and (2) are useful when describing the $\gamma$-ray behavior, they do not reproduce correctly the peak position $E_\gamma^{\max}$ [27]. The simulation software uses Eq. (12) and the reference frame transformations discussed in Sec. IV.A, which accounts for all the various kinematic factors like the energy spread $\delta E_e$, the angle smearing $\sigma'$, and the crossing angle $\delta$. Therefore, $E_\gamma^{\max}$ is in practice set by adjusting $E_e$ until the corresponding Fig. 6 has the peak at zero. Values different by 0.6%–1.4% than those given by Eq. (2) are obtained for $E_e$.

Three specification parameters have simple dependencies on the collimation aperture $a$. The beam spot is linearly proportional to the aperture $D_x \approx 0.9a$, which implies that $D_\theta \approx 0.9a/10$ m, hence the requirement from Table I is met for any $a < 1.66$ mm. For the collimation angles below 80 μrad used here, the mean $\gamma$ linear polarization $\xi$ is equal to the laser linear polarization and has the RMS below $10^{-4}$. Finally, off-peak spectral densities OSD well below the specification required in Table I were obtained. Obviously, being a parameter that quantifies the background level in the $\gamma$ beam spot, the experimental verification of its magnitude is mandatory during the VEGA beamline commissioning.

A systematic study of the main $\gamma$ beam specifications BW, $F$, and SD as function of the collimator aperture $a$ is shown in Fig. 7. They are extracted from the energy spectra after collimation, like those in Figs. 5 and 6. Specifically, BW $= 100 \times \mathrm{FWHM}/E_\gamma^{\max}$, $F$ is the integral normalized to $I = 10^{11}$ $\gamma$/s, and SD $= F/\mathrm{FWHM}$. Parameters for the green laser are shown in green, while those for the IR laser are displayed in red. The symbols show the electron energy: circles for 528 MeV, squares for 647 MeV, and crosses for 747 MeV. The resulting $E_\gamma^{\max}$ values for each ($\lambda$, $E_e$) combination are given in the two legends. In order to better visualize the dependencies, data points are joined with smoothed curves. Finally, the desired specification ranges from Table I are displayed with purple dotted lines and arrows.

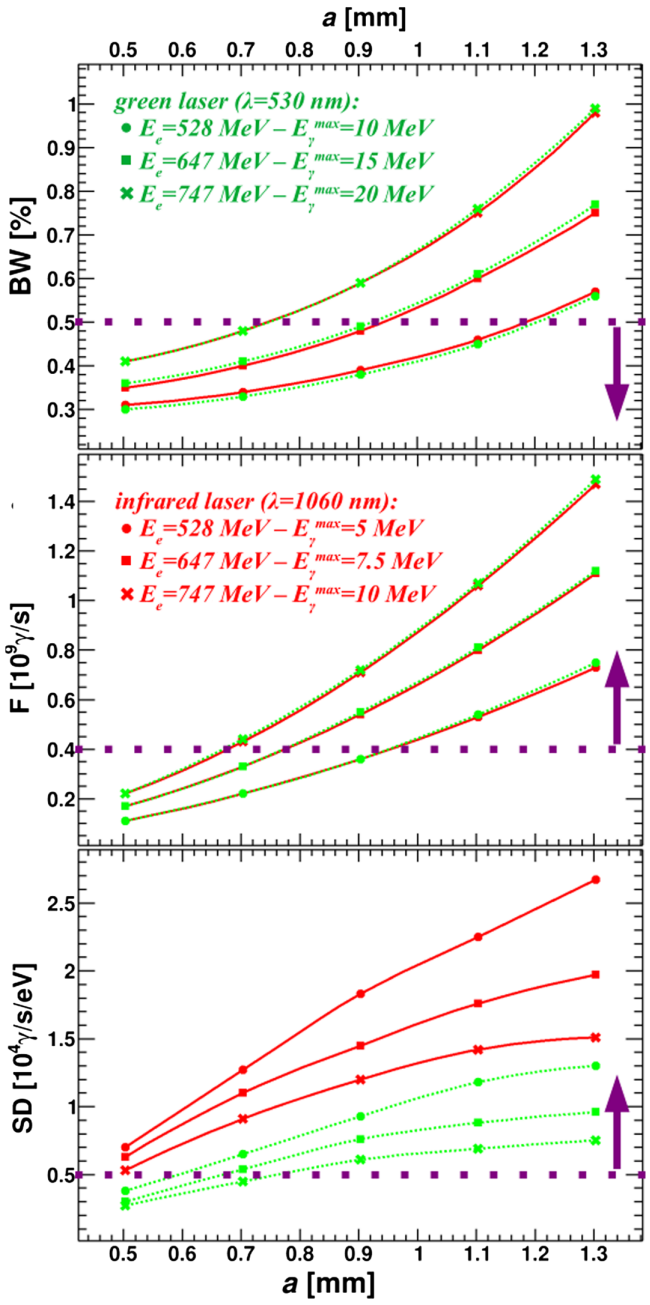


FIG. 7. Bandwidth BW, flux $F$, and spectral density SD dependence on the collimation aperture $a$ in the top, middle, and bottom panels, respectively. The meaning of colors and symbols is given in the legends. The dotted purple lines and the purple arrows show the specifications from Table I. The curves join the data points and are not fits.

Related to the energy dependence in Fig. 7, the top and middle panels demonstrate how doubling the laser wavelength generates the same BW and $F$ parameters for half the $\gamma$ energy, while the bottom panel shows that SD increases as either $E_e$ or $E_l$ decreases. Fits of BW($a$) with functions quadratic in aperture reveal, after the conversion of $a$ to $\theta_{\rm coll}$ and of FWHM to rms, a good description by $\mathrm{BW}(\theta_{\rm coll}) \approx \gamma_e^2\theta_{\rm coll}^2/\sqrt{12}$. According to Eq. (9), this implies that, for the input parameters in Table III, the $\gamma$ bandwidth is indeed dominated by the setting of the collimation system. The flux is also well described by a quadratic dependence on the aperture $F(a) \approx sa^2$ but with higher slopes $s$ than BW. Finally, SD grows slowly with $a$ and saturates.

Establishing the optimal collimation aperture for a particular experimental program depends on its specific requirements. For example, giant dipole resonance studies, which cover several MeVs and as such allow for bandwidths up to 10%, require a flux as high as possible in a beam spot limited by the target production technologies. Alternatively, pygmy dipole resonance studies in the high level density region require very low bandwidth, even if it must come at the expense of low flux. Nonetheless, the most nuclear physics programs attempt to balance narrow bandwidths against high fluxes. Then the ratio of the two, namely the spectral density, becomes the figure of merit for an optimal $\gamma$ beamline.

Applying the specifications in Table I to the six beamlines in Fig. 7 gives the following solutions: (i) $a = 1.1$ mm for $E_\gamma = 5$ MeV; (ii) $a = 0.9$ mm for $E_\gamma = 7.5$ MeV; (iii) $a = 0.7$ mm for $E_\gamma = 10$ MeV with the IR laser; (iv) $a = 1.1$ mm for $E_\gamma = 10$ MeV with the green laser; (v) $a = 0.9$ mm for $E_\gamma = 15$ MeV; and (vi) $a = 0.7$ mm for $E_\gamma = 20$ MeV.

Actually, the strict enforcement of the specifications in Table I gives no solution for the 20 MeV beamline. The $a$ value in this case is found only if $P_L$ is increased by ~10%, corresponding to an intensity $I = 1.1 \times 10^{11}$ $\gamma$/s.

## VI. GAMMA BEAMLINE SENSITIVITY TO PARAMETER VARIATIONS

A set of input parameters for the electron and laser beams are proposed in Sec. III, in order to obtain the VEGA specifications described in Sec. II. After demonstrating how these specifications are met in Sec. V, the last remaining study is to vary these parameters and assess the sensitivity of $\gamma$-ray beam parameters, namely of BW, $F$, and SD, to their value. The parameters of the incoming beams with the largest potential impact are $\epsilon$, $\beta$, $\beta_0$, and $\alpha$.

The units used throughout this section in all distributions and fit functions are: BW in %, $F$ in $10^9$ $\gamma$/s, SD in $10^4$ $\gamma$/s/eV, $\epsilon$ in nm, $\beta$ and $\beta_0$ in m. If the parameters being varied change the total intensity, each collimated energy spectrum used to extract the $\gamma$ beamline parameters is scaled to its corresponding $I$ value. The case analyzed is that of the 20 MeV beamline, hence $E_e = 747$ MeV, $\lambda = 530$ nm, $a = 0.7$ mm, and $\theta_{\rm coll} = 38$ μrad.

It has been argued in Sec. III that, for the chosen energy range of the electron beam, the emittance variation due to effects like IBS and adiabatic damping should be moderate. Moreover, the impact of emittance variation on the $\gamma$-ray beam is *a priori* obvious: the smaller and

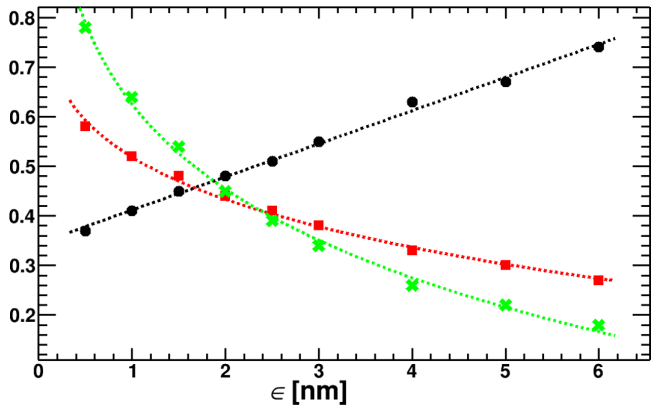


FIG. 8. BW (black circles), $F$ (red squares), and SD (green crosses) dependence on ESR emittance at the IP for the 20 MeV $\gamma$ beamline. The fits are shown with dashed lines.

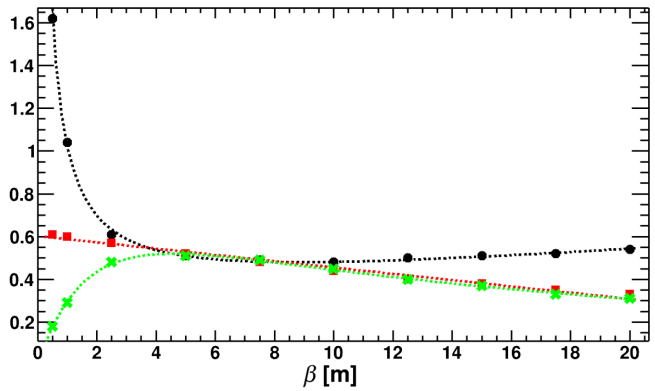


FIG. 9. BW (black circles), $F$ (red squares), and SD (green crosses) dependence on ESR beta function at the IP for the 20 MeV $\gamma$ beamline. The fits are shown with dashed lines.

the better. Nonetheless, emittance at the IP is the most important ESR parameter, so the study starts with it.

The dependence of the 20 MeV $\gamma$ beamline parameters on the ESR emittance at the IP, shown in Fig. 8, is parameterized by the following fit functions:

$$\begin{aligned} \mathrm{BW}(\epsilon) &= 0.345 + 0.067\epsilon, \\ F(\epsilon) &= 1.118 - 0.599\epsilon^{0.191}, \\ \mathrm{SD}(\epsilon) &= 4.258 - 3.632\epsilon^{0.067}. \end{aligned} \tag{14}$$

The BW linear dependence results from Eq. (9), where the intercept is composed of $2\delta E_e/E_e = 0.1\%$ and $\gamma_e^2\theta_{\mathrm{coll}}^2/\sqrt{12} = 0.09\%$, while the slope is equal to $2\gamma_e^2/\beta = 0.04\%/\mathrm{nm}$. Converted from rms to FWHM, a value close to the fit intercept is obtained, while the calculated slope is about 40% higher than the fit. Note, however, that the spectra after collimation are not Gaussian, hence the above conversion is approximate. As expected, $F$ and SD drop with $\epsilon$, with the latter being particularly sensitive to emittance variations.

The impact of the beta function variation is difficult to assess *a priory*, as discussed in Sec. II. Indeed, Fig. 9 presents an interesting behavior, described by the following fit functions:

$$\begin{aligned} \mathrm{BW}(\beta) &= (0.832 + 0.189\beta + 0.0038\beta^2)/\beta^{0.809}, \\ F(\beta) &= 0.603 - 0.0147\beta, \\ \mathrm{SD}(\beta) &= \beta^{1.012}/(2.328 + 0.920\beta + 0.116\beta^2). \end{aligned} \tag{15}$$

Using again Eq. (9), a $1/\beta$ divergence of the bandwidth should be expected at low values. Coupled with the mild decrease of $F$, it drives SD toward 0 in this region. The optimal interval for bandwidth and spectral density is $\beta \sim 5$–$7$ m. Values below 2 m should be avoided for this beamline as they lead to very poor $\gamma$-ray properties, unless the interest is only for flux maximization.

The dependence on $\beta_0$ has been checked and only the total intensity varies, according to Eqs. (4) and (10). All other $\gamma$ beamline parameters proportional with $I$, like $F$ and SD, have the dependency on $\beta_0$ that comes only through $I$.

One of the simplifying assumptions made when defining the ESR parameters was that there is no transversal position-angle correlation at the IP location $s_0$, hence $\alpha(s_0) = 0$. Since this parameter is not negligible at any ESR, the impact of its variation needs to be assessed. Its increase in the interval (0,1) leads to a very slow BW decrease and SD increase, while $F$ remains constant. The fit functions for the 20 MeV beamline are

$$\begin{aligned} \mathrm{BW}(\alpha) &= 0.480 - 0.109\alpha + 0.040\alpha^2, \\ F(\alpha) &= 0.44, \\ \mathrm{SD}(\alpha) &= 0.448 + 0.166\alpha - 0.085\alpha^2, \end{aligned} \tag{16}$$

where $\alpha$ is unitless. For example, a significant increase of $\alpha$ from 0 to 0.5 decreases BW from 48% to 44% and increases SD from $4.9 \times 10^3$ to $5.1 \times 10^3$ $\gamma/\mathrm{s/eV}$.

Other parameters of the two beams can have a significant impact of the $\gamma$-ray properties, but their study implies precise knowledge on the electron and photon optics used to focus them at the IP. An example is the electron dispersion function. Their study is left for future work on the ESR and ROC design.

## VII. SUMMARY AND OUTLOOK

The general design concept for the VEGA facility at ELI-NP was described, including the specifications for its $\gamma$-ray beam and the proposed parameters of the electron and laser beams at their interaction point which generate these specifications. A simulation program was used to study the properties of the $\gamma$ beamline, optimize its settings, and assess its sensitivity to parameter variations.

This work will be followed by the design of the electron linear accelerator and storage ring and of the laser optical

cavity that meets the properties at the interaction point proposed here. A future publication will then be able to address in more detail specific issues, like the magnitude of the intrabeam scattering and synchrotron radiation effects, effects of electron, and laser focusing optics, and present technical solutions for an optimal $\gamma$-ray beam.

Future upgrades of the VEGA facility, such as the use of a laser wavelength of around 2120 nm or an additional laser for radiative beam cooling in order to reach lower gamma energies, the increase in optical cavity power for higher $\gamma$ source intensity, and the inclusion of a circularly polarized laser will also be considered.

## ACKNOWLEDGMENTS

P. C. would like to thank G. Suliman for the fruitful discussions on the software implementation of the Compton scattering process. This work was carried out under the contract PN 23 21 01 06 sponsored by the Romanian Ministry of Research, Innovation, and Digitalization.

## APPENDIX: MONTE CARLO ALGORITHM FOR GAMMA GENERATION AT THE IP

The *GammaGenerator* class starts by generating an electron described by the *G4ThreeVector* position

$$\begin{aligned} x &= \sqrt{2\mathcal{E}_1\epsilon\beta}\cos\mathcal{U}_1, \\ y &= \sqrt{2\mathcal{E}_2\epsilon\beta}\cos\mathcal{U}_2, \\ z &= \sigma_z\mathcal{G}(0,1), \end{aligned} \tag{A1}$$

and the *G4LorentzVector* 4-momentum

$$\begin{aligned} E &= \mathcal{G}(E_e, E_e\delta E_e) + m_e c^2, \\ P_z &= \sqrt{\frac{E_e^2 - (m_e c^2)^2}{1 + x'^2 + y'^2}}, \\ P_y &= P_z y', \\ P_x &= P_z x', \end{aligned} \tag{A2}$$

with the transversal angular components

$$\begin{aligned} x' &= -\sqrt{2\mathcal{E}_1\epsilon/\beta}(\alpha\cos\mathcal{U}_1 + \sin\mathcal{U}_1), \\ y' &= -\sqrt{2\mathcal{E}_2\epsilon/\beta}(\alpha\cos\mathcal{U}_2 + \sin\mathcal{U}_2), \end{aligned} \tag{A3}$$

and the following random numbers: $\mathcal{E}_{1,2}$ with exponential distribution of mean 1, $\mathcal{U}_{1,2}$ with uniform distribution in $(0, 2\pi)$, and $\mathcal{G}(m, w)$ with Gaussian distribution of mean $m$ and width $w$. All the other parameters describe the electron beam at the IP and have been defined throughout the article. The boost vector $\vec{b}$ is obtained with the $boostVector()$ method of the electron *G4LorentzVector*.

The laser photon is generated at the same position $(x, y, z)$ as the electron and with the *G4LorentzVector* 4-momentum

$$\begin{aligned} E_l &= 2\pi\hbar c/\lambda, \\ P_x &= -\frac{E_l c_1}{\sqrt{1 + c_1^2 + c_2^2}}, \\ P_y &= -\frac{E_l c_2}{\sqrt{1 + c_1^2 + c_2^2}}, \\ P_z &= -\frac{E_l}{\sqrt{1 + c_1^2 + c_2^2}}, \end{aligned} \tag{A4}$$

with the coefficients

$$c_1 = \frac{xz}{z^2 + \beta_0^2}, \qquad c_2 = \frac{yz}{z^2 + \beta_0^2}. \tag{A5}$$

A rotation with the crossing angle $\delta$ and the initialization of the polarization finish the laser photon definition.

The next step is to transform these vectors to the electron rest frame by boosting them with $-\vec{b}$ and align the photon on the positive $z$ axis. In this reference frame, all the equations are much simpler, like the energy-angle Eq. (12) or the energy and angle differential cross sections. Specifically, the energy differential cross section is

$$\begin{aligned} \frac{\mathrm{d}\sigma}{\mathrm{d}E_\gamma} &= C(E_l)P(E_l, E_\gamma), \\ P(E_\gamma) &\equiv \frac{u^2 + 2u + v}{2(1 + E_l/m_e c^2)} \\ u &\equiv \frac{m_e c^2}{E_l} - \frac{m_e c^2}{E_\gamma}, \qquad v \equiv \frac{E_l}{E_\gamma} + \frac{E_\gamma}{E_l}, \end{aligned} \tag{A6}$$

where $P(E_\gamma)$ contains the $E_\gamma$ dependence and fulfills $0 \le P(E_\gamma) \le 1$, hence it can be used as $E_\gamma$ probability distribution. Similarly, the $\phi_\gamma$ probability distribution is extracted from the azimuthal differential cross section:

$$P(\phi_\gamma) = \frac{1}{\pi}\frac{[1 + P_l\cos 2(\phi_l - \phi_\gamma)](u^2 + 2u) + v}{2(u^2 + 2u) + v}, \tag{A7}$$

where $P_l$ and $\phi_l$ are the laser degree and angle of linear polarization in the electron laboratory frame.

Using the above probability distributions, the emitted $\gamma$ is generated with the following algorithm: (1) generate random $E_\gamma$ uniformly in the interval

$$\frac{E_l}{1 + 2E_l/m_e c^2} \le E_\gamma \le E_l \tag{A8}$$

resulting from $|\cos\theta_\gamma| \le 1$ applied to Eq. (12); (2) generate random $r_1$ uniformly in the interval [0, 1]; (3) if $r_1 \le P(E_\gamma)$,

accept $E_\gamma$ and move to next step; otherwise, return to step 1; (4) insert $E_\gamma$ in Eq. (12) to compute $\theta_\gamma$; (5) generate random $\phi_\gamma$ uniformly in the interval $[0, 2\pi]$; (6) generate random $r_2$ uniformly in the interval [0, 1]; (7) if $r_2 \leq P(\phi_\gamma)$, accept $\phi_\gamma$ and move to next step; otherwise, return to step 5; (9) calculate the linear component of the Stokes vector:

$$\xi = P_l\left(1 - \frac{u^2}{2(u^2 + 2u + v)}\right). \tag{A9}$$

Finally, the resulting gamma is boosted back to the laboratory frame with vector $\vec{b}$.


[1] K. A. Tanaka *et al.*, Current status and highlights of the ELI-NP research program, Matter Radiat. Extremes **5**, 024402 (2020).

[2] D. Doria, M. O. Cernaianu, P. Ghenuche, D. Stutman, K. A. Tanaka, C. Ticos, and C. A. Ur, Overview of ELI-NP status and laser commissioning experiments with 1 PW and 10 PW class-lasers, J. Instrum. **15**, C09053 (2020).

[3] A. Zilges, D.L. Balabanski, J. Isaak, and N. Pietralla, Photonuclear reactions—From basic research to applications, Prog. Part. Nucl. Phys. **122**, 103903 (2022).

[4] VEGA Technical Design Report, 2022 (unpublished).

[5] C. A. Ur *et al.*, Nuclear resonance fluorescence experiments at ELI-NP, Rom. Rep. Phys. **68**, S483 (2016), https://rrp.nipne.ro/2016_68_S.html.

[6] F. Camera *et al.*, Gamma above the neutron threshold experiments at ELI-NP, Rom. Rep. Phys. **68**, S539 (2016), https://rrp.nipne.ro/2016_68_S.html.

[7] O. Tesileanu *et al.*, Charged particle detection at ELI-NP, Rom. Rep. Phys. **68**, S699 (2016), https://rrp.nipne.ro/2016_68_S.html.

[8] D. L. Balabanski *et al.*, Photofission experiments at ELI-NP, Rom. Rep. Phys. **68**, S621 (2016), https://rrp.nipne.ro/2016_68_S.html.

[9] M. Bobeica *et al.*, Radioisotope production for medical applications at ELI-NP, Rom. Rep. Phys. **68**, S847 (2016),https://rrp.nipne.ro/2016_68_S.html.

[10] G. Suliman *et al.*, Gamma-beam industrial applications at ELI-NP, Rom. Rep. Phys.**68**, S799 (2016),https://rrp.nipne.ro/2016_68_S.html.

[11] N. Djourelov *et al.*, Positron production by gamma beam at ELI-NP, Rom. Rep. Phys. **68**, S735 (2016), https://rrp.nipne.ro/2016_68_S.html.

[12] H. R. Weller, M. W. Ahmed, H. Gao, W. Tornow, Y. K. Wu, M. Gai, and R. Miskimen, Research opportunities at the upgraded HI$\gamma$S facility, Prog. Part. Nucl. Phys. **62**, 257 (2009).

[13] Z. R. Hao *et al.*, Collimator system of SLEGS beamline at Shanghai Light Source, Nucl. Instrum. Methods Phys. Res., Sect. A **1013**, 165638 (2021).

[14] H. Utsunomiya *et al.*, The $\gamma$-ray beam-line at NewSUBARU, Nucl. Phys. News **25**, 25 (2015).

[15] N. Muramatsu *et al.*, Development of high intensity laser-electron photon beams up to 2.9 GeV at the SPring-8 LEPS beamline, Nucl. Instrum. Methods Phys. Res., Sect. A **737**, 184 (2014).

[16] B. Szpunar, C. Rangacharyulu, S. Daté, and H. Ejiri, Estimate of production of medical isotopes by photo-neutron reaction at the Canadian Light Source, Nucl. Instrum. Methods Phys. Res., Sect. A **729**, 41 (2013).

[17] D. Babusci *et al.*, Project GRAAL: The scientific case, Il Nuovo Cimento A **103**, 1555 (1990).

[18] G. Ya. Kezerashvili, A. M. Milov, N. Yu. Muchnoi, and A. P. Usov, A Compton source of high energy polarized tagged $\gamma$-ray beams. The ROKK-1M facility, Nucl. Instrum. Methods Phys. Res., Sect. B **145**, 40 (1998).

[19] C. Sun *et al.*, Energy and energy spread measurements of an electron beam by Compton scattering method, Phys. Rev. ST Accel. Beams **12**, 062801 (2009).

[20] N. Ranjan, B. Terzić, G. A. Krafft, V. Petrillo, I. Drebot, and L. Serafini, Simulation of inverse Compton scattering and its implications on the scattered linewidth, Phys. Rev. Accel. Beams **21**, 030701 (2018).

[21] A. Wolski, Low-emittance storage rings, arXiv:1507.02213.

[22] H. Wiedemann, *Particle Accelerator Physics* (Springer International Publishing AG, Switzerland, 2019).

[23] Z. Huang and R. D. Ruth, Laser-electron storage ring, Phys. Rev. Lett. **80**, 976 (1998).

[24] G. Paterno, P. Cardarelli, M. Bianchini, A. Taibi, I. Drebot, V. Petrillo, and R. Hajima, Generation of primary photons through inverse Compton scattering using a Monte Carlo simulation code, Phys. Rev. Accel. Beams **25**, 084601 (2022).

[25] C. Sun and Y. K. Wu, Theoretical and simulation studies of characteristics of a Compton light source, Phys. Rev. ST Accel. Beams **14**, 044701 (2011).

[26] W. J. Brown and F. V. Hartemann, Three-dimensional time and frequency-domain theory of femtosecond x-ray pulse generation through Thomson scattering, Phys. Rev. ST Accel. Beams **7**, 060703 (2004).

[27] G. A. Krafft, E. Johnson, K. Deitrick, B. Terzić, R. Kelmar, T. Hodges, W. Melnitchouk, and J. R. Delayen, Laser pulsing in linear Compton scattering, Phys. Rev. Accel. Beams **19**, 121302 (2016).

[28] K. Deitrick, G. H. Hoffstaetter, C. Franck, B. D. Muratori, P. H. Williams, G. A. Krafft, B. Terzić, J. Crone, and H. Owen, Intense monochromatic photons above 100 keV from an inverse Compton source, Phys. Rev. Accel. Beams **24**, 050701 (2021).

[29] R. Hajima, Bandwidth of a Compton radiation source with an electron beam of asymmetric emittance, Nucl. Instrum. Methods Phys. Res., Sect. A **985**, 164655 (2021).

[30] K. Yokoya, *CAIN User Manual v2.35* (KEK, Japan, 2003).

[31] S. Agostinelli, GEANT4-a simulation toolkit, Nucl. Instrum. Methods Phys. Res., Sect. A **506**, 250 (2003).

[32] CLHEP—A class library for high energy physics, https://proj-clhep.web.cern.ch.

[33] G. Suliman, ELI-NP internal note, ELI-NP/RA4/01, 2015.

[34] W. Hillert, Transverse linear beam dynamics, arXiv:2107.02614.

[35] G. Paterno *et al.*, A collimation system for ELI-NP Gamma Beam System—Design and simulation of performance, Nucl. Instrum. Methods Phys. Res., Sect. B **402**, 349 (2017).

[36] H. Carstens *et al.*, Megawatt-scale average-power ultrashort pulses in an enhancement cavity, Opt. Lett. **39**, 2595 (2014).

[37] M. A. Furman, The hourglass reduction factor for asymmetric colliders, SLAC, Technical Report No. ABC-41, 1991.

[38] G. A. Krafft, B. Terzić, E. Johnson, and G. Wilson, Scattered spectra from inverse Compton sources operating at high laser fields and high electron energies, Phys. Rev. Accel. Beams **26**, 034401 (2023).

[39] M. Pisharody, P. K. Job, S. Magill, J. Proudfoot, and R. Stanek, Measurement of gas bremsstrahlung from electron storage rings, Nucl. Instrum. Methods Phys. Res., Sect. A **401**, 442 (1997).